# Grid-Based Kinetic Simulations of Collisionless Plasma Expansion

**IEPC-2019-862**

*Presented at the 36th International Electric Propulsion Conference*
*University of Vienna, Austria*
*September 15-20, 2019*

Chen Cui,*Ziyu Huang,†Yuan Hu,‡Joseph Wang§
*University of Southern California, Los Angeles, CA, 90089, USA*

**Previous fully kinetic PIC simulations showed that the electrons in the plasma plume emitted from electric propulsion thrusters are non-equilibrium and the electron temperature is anisotropic. To further study the electron kinetic properties in plasma expansion and to reduce the interference from numerical noise in particle simulations, this study presents a grid-based Vlasov method model. This model is benchmarked against particle-in-cell simulations and analytical solutions on semi-infinite collisionless plasma expansion and finite-size collisionless plasma expansion. It is shown that the Vlasov model captures the same anisotropic kinetic characteristics observed in previous full PIC simulation results and eliminates the interference from the typical numerical noise in a PIC model.**

## I. Introduction

ELECTRIC thruster plume is a fundamental problem in electric propulsion (EP), and has been investigated extensively. The propellant beam ions and neutralizing electrons from ion and Hall thrusters form a mesothermal plasma flow with $v_{ti} \ll v_d \ll v_{te}$, where $v_{ti}$, $v_d$ and $v_{te}$ are the ion thermal velocity, beam velocity, and electron thermal velocity, respectively. For typical EP application problems, the plume can be considered collisionless as the collision mean free path is much larger than the plume characteristic length.

Most EP plume simulation models are based on the hybrid particle-in-cell (PIC) method.[1–4] In a hybrid PIC model, the ions are modeled as macroparticles while the electrons are modeled as an equilibrium massless fluid to save on computational time. A common approach is to treat the electrons as a massless, isothermal, ideal gas. From the electron state equation and momentum equation, one obtains the Boltzmann relation between the electron density $n_e$ and the electric potential $\Phi$:

$$n_e = n_0 \exp\left[\frac{e(\Phi - \Phi_0)}{k_b T_{e0}}\right], \tag{1}$$

where $n_0$, $\Phi_0$ and $T_{e0}$ are the plume density, potential and electron temperature at thruster exit, respectively. Eq (1) has been used in almost all plasma plume simulation models so far. However, recent fully kinetic PIC simulation studies by Hu and Wang[5–7]showed that the electrons in a plasma plume are highly non-equilibrium and the electron temperature is anisotropic. Hence, neither the Boltzmann relation, eq(1), nor the more general polytropic law appears to be a good assumption for modeling electrons in plasma plumes.

The work presented here is part of an ongoing study that extends the previous work of Hu and Wang[5–7] to further investigate the kinetic characteristics in collisionless mesothermal plasma plume expansion. A major limitation in any PIC model is the inherent statistical noise. In particular, the statistical noise due to insufficient number of macro-particles interferes with the analysis of the thermodynamics and energy flow

*Ph.D. Student, Department of Astronautical Engineering, cuichen@usc.edu
†Ph.D. Student, Department of Astronautical Engineering, ziyuhuan@usc.edu
‡Currently Research Professor, Institute of Mechanics, Chinese Academy of Sciences, Beijing, China, yhu@imech.ac.cn
§Professor, Department of Astronautical Engineering, josephjw@usc.edu

in a collisionless plasma flow. Hence, we are motivated to explore an approach other than PIC so to reduce the numerical noise. This paper develops a grid-based fully kinetic simulation model.

Plasma expansion is also a classical problem that has been studied extensively theoretically. Previous theoretical/analytical studies include 1-D semi-infinite plasma expansion[8–13] and 1-D finite-size plasma expansion.[14–22] Under the quasi-neutral isothermal assumption and using a fluid model for both the ions and electrons, the semi-infinite plasma expansion can be described by the self-similar solution.[8,9] Mora and Pellat[12] treated the electrons kinetically and found that the self-similar solution is a zeroth-order approximate solution. For the finite-size plasma expansion problem, theoretical studies showed that the electron temperature is strongly inhomogeneous and the expansion drives the electron velocity distribution function towards a non-Maxwellian distribution. Hu and Wang[7] showed that the plasma plume expansion expansion process in the axial direction is analogous to a semi-infinite plasma expansion and that in the radial direction is analogous to a finite-size plasma expansion. Hence, in this paper, we use 1-D semi-infinite plasma expansion and finite-size plasma expansion as benchmark applications to validate the numerical code.

## II. Simulation Model

The Vlasov equation provides the general kinetic description of a collisionless plasma system. Here, we consider an unmagnetized, collisionless plasma:

$$\frac{\partial f_\alpha}{\partial t} + \boldsymbol{v} \cdot \nabla_{\boldsymbol{x}} f_\alpha + \boldsymbol{a} \cdot \nabla_{\boldsymbol{v}} f_\alpha = 0 \tag{2}$$

where $f_\alpha(x, v, t)$ is the velocity distribution function. The acceleration term in equation 2 is

$$\boldsymbol{a} = \frac{F_\alpha}{m_\alpha} = \frac{q_\alpha \cdot \boldsymbol{E}}{m_\alpha} = \frac{-q_\alpha \nabla \Phi}{m_\alpha} \tag{3}$$

The electric potential. $\Phi$ needs to be solved self-consistently using the Poisson equation

$$\nabla \cdot (\epsilon_0 \nabla \Phi) = -e(Z_i n_i - n_e) \tag{4}$$

where $Z_i$, $n_i$, and $n_e$ denote the charge number, ion number density, and electron number density, respectively. The macroscopic properties of the system are described by moments of the velocity distribution function

$$< M_n >= \int_{-\infty}^{\infty} M_n \hat{f} d\boldsymbol{v} \tag{5}$$

The general numerical approach to solve the Vlasov equation may be classified into two different types of methods. The first one is the particle-based method. The particle method uses the Lagrangian scheme and solve the Eq (2) by tracking the trajectories of macro particles. The physical variables and information are obtained from the statistics of particles' information. PIC falls into this category. The particle method is easy to implement and but may suffer from inherent numerical noise. The second one is the grid-based method. The grid-based method directly solves Eq (2) for the velocity distribution in the discrete phase space. This method has no inherent statistical noise. However, comparing to PIC, the numerical implementation is more involved and computational cost is typically much higher.

### A. Numerical Scheme

While the Vlasov-Poisson system is a non-linear system, the Vlasov equation itself is a first-order hyperbolic partial differential equation (PDE). Many numerical schemes have been developed to solve hyperbolic PDEs. The numerical schemes may be divided into two categories. The first one is splitting the dimensions so to make the Vlasov equation a group of linear advection partial differential equations.[23,24] The second one is unsplitted methods.[25,26] The semi-Lagrangian method is broadly used for the first category and the Full-Eulerian method is broadly used for the second one. The finite difference,[27] finite volume,[28,29] finite element[30] methods are used to discrete the phase spaces. While the grid-based Vlasov simulation method has been mostly used by the fusion[31,32] and astrophysics community,[33,34] it was applied in several EP studies recently.[35,36]

In our simulation the simulation method need to fulfill several properties. The conservation of the flux and average need to be guaranteed:

$$\int_{x_{i-1/2}}^{x_{i+1/2}} f_h(x) = \Delta x \cdot f_i \tag{6}$$

Since the distribution function is always positive, the scheme needs to ensure that:

$$0 \leq f_h(x) \leq f_\infty, \ where \ f_\infty = max_{j \in I} f_j \tag{7}$$

$$f_h(x) \geq 0, \ f(x) \geq 0 \tag{8}$$

The numerical scheme used in this work is the Positive Flux Conservation (PFC) method.[28] This method can satisfy all of the requirements mentioned above and achieve an up to fifth order accuracy.[29,37] The PFC scheme used in our simulation is chosen to be the third-order one to balance the accuracy requirement and the computational cost.

The Vlasov equation under the PFC scheme can be written into the following conservation form:

$$\int_{x_{i-1/2}}^{x_{i+1/2}} f(t^{n+1}, x)dx = \Psi_{i-1/2}(t^n) + \int_{x_{i-1/2}}^{x_{i+1/2}} f(t^n, x)dx - \Psi_{i+1/2}(t^n) \tag{9}$$

where the $\Psi$ is defined as the numerical flux:

$$\Psi_{i+1/2}(t^n) = \int_{X(t^n, t^{n+1}, x_{i+1/2})}^{x_{i+1/2}} f(t^n, x)dx \tag{10}$$

In Eq (9), the term $X(t^n, t^{n+1}, x_{i+1/2})$ is the start at time $t^n$ level of a characteristic line with an end as $x_{i+1/2}(t^{n+1})$. Details of how to construct the numerical flux $\Psi$ can be found in Filbet's work.[28]

The boundary condition for Vlasov equation in this work is the fixed boundary condition in the spatial space. In the velocity space, the so-called "cut-off" boundary condition is applied. A sufficiently large velocity is selected to ensure that the velocity distribution function approaches zero(in this work selected to be $1 \times 10^{-12}$) at the boundary. Thus the boundary condition given in velocity space is a zero-value Dirichlet boundary condition. One also needs to ensure that the plasma "particles" can not travel more than one grid cell in both spatial space and velocity space. Thus although the PFC scheme does not need the CFL condition itself, in practice we need to ensure the CFL condition.

$$\begin{cases} \frac{v_{max} dt}{dx} \leq 1 \\ \frac{a_{max} dt}{dv} \leq 1 \end{cases} \tag{11}$$

Thus the time step need to be chosen carefully for the grid cell size.

### B. Simulation Setup

All of variables in the simulation model are normalized respect to the electron parameters at initial time moment's phase space. The Debye length is defined to be $\lambda_{D0} = \sqrt{\epsilon_0 k_b T_{e0}/n_0 e^2}$ and the electron plasma frequency at the initial moment is defined to be $\omega_{pe0} = \sqrt{n_0 e^2/\epsilon_0 m_e}$ . The thermal velocity of electrons is defined to be $v_{te0} = \sqrt{k_b T_{e0}/m_e}$. Ion acoustic velocity is defined to be $C_{s0} = \sqrt{k_b T_{e0}/m_i}$. In all of the equations mentioned above the subscript "0" means the value is at the initial moment's phase space. According to the variables defined above we can define the normalization scheme which is shown below:

$$\begin{cases} \tilde{\boldsymbol{x}} = \frac{\boldsymbol{x}}{\lambda_{D0}} \\ \tilde{t} = t\omega_{pe0} \\ \tilde{m} = \frac{m}{m_e} \\ \tilde{v}_\alpha = \frac{v_\alpha}{v_{te0}} \\ \tilde{n}_\alpha = \frac{n_\alpha}{n_{e0}} \\ \tilde{\Phi} = \frac{e\Phi}{k_b T_{e0}} \\ \tilde{f} = \frac{f}{n} \cdot v_{te0} \end{cases} \tag{12}$$

In this paper, two simulation setups are considered. Specifically, we consider a semi-infinite plasma expansion into a vacuum and a finite-size expansion with a plasma loaded initially. The parameters are chosen such that the plasma is mesothermal. The ion to electron mass ratio is taken to be 100 in both the semi-infinite expansion simulation and the finite-size expansion simulation. The initial ratio of the temperature is taken to be $T_i/T_e = 0.01$. The Mach number is set to be 4.0, similar to the typical beam velocity of ion thruster plume. The Mach number for the finite-size model is set to be zero to represent the radial plasma expansion of the plume. Other relevant parameters for the semi-infinite and finite-size plasma expansion simulations are shown in Table 1.

Table 1: Normalized Plasma Parameters for Semi-infinite and (Finite-size) Expansion Simulation

| $m_i/m_e$ | $T_{i0}/T_{e0}$ | $v_{ti0}/v_{te0}$ | $v_d/v_{te0}$ | $C_{s0}/v_{te0}$ | $Ma$ |
|---|---|---|---|---|---|
| 100.0 | 0.01 | 0.01 | 0.4(0) | 0.1(0) | 4.0(0) |

Both the electrons and ions follow the Maxwellian velocity distribution initially. In the semi-infinite expansion simulation, the plasma is loaded at the left-hand side domain as shown in figure 1. In the finite-size expansion simulation, the plasma is preloaded in the center of the domain as shown in figure 2. The size of the pre-loaded plasma is $10\lambda_{D0}$.

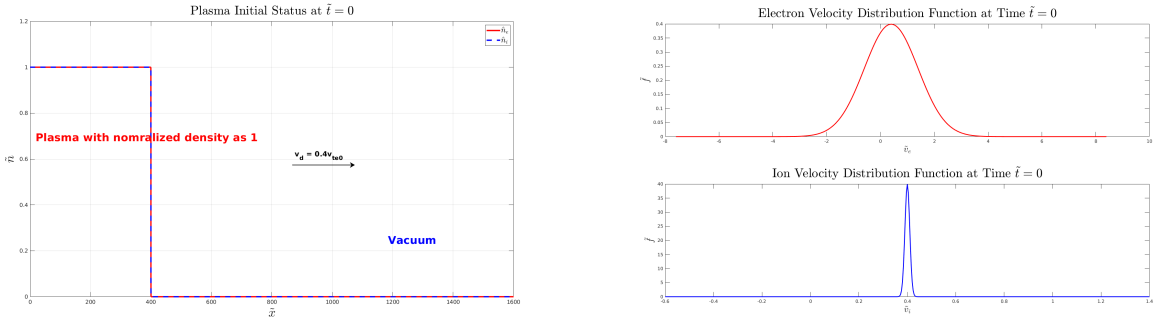


(a) Initial Plasma Spatial Distribution

(b) Initial Plasma Velocity Distribution

Figure 1: Semi-Infinite Plasma Initial Status

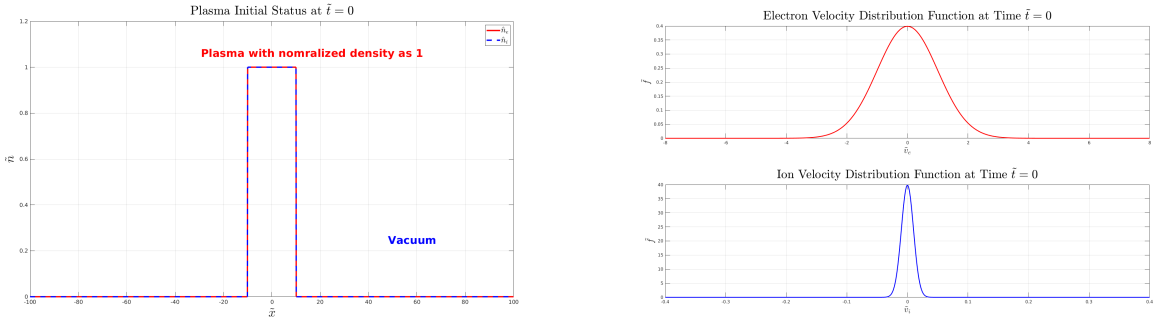


(a) Initial Plasma Spatial Distribution

(b) Initial Plasma Velocity Distribution

Figure 2: Finite-Size Plasma Initial Status

The simulation domain is a 1-D spatial space and 1-D velocity space(1D1V). The domain size is selected to guarantee that the expansion front is still far from boundary after the expansion is well established. The discretization of the velocity space need to be careful. It is important to choose the velocity cut-off limit in the velocity space to avoid truncation errors. The computational domain/time parameters are listed in Table 2. The boundary conditions are summarized in Table 3. The simulation is run through 400 electron periods (40 ion periods).

Table 2: Simulation Domain/Time Parameters for Semi-infinite and (Finite-size) Expansion Simulation

| | Length | Cells | Left Bound | Right Bound | Total Time | Time Step Size |
|---|---|---|---|---|---|---|
| X | $1600\lambda_{D0}$ | 8000 | 0 | $1600\lambda_{D0}$ | $t\omega_{pe0} = 400$ | $\Delta t\omega_{pe0} = 0.025(0.01)$ |
| Electron | $16v_{te0}$ | 256 | $-7.6v_{te0}(-8v_{te0})$ | $8.4v_{te0}(8v_{te0})$ | $t\omega_{pe0} = 400$ | $\Delta t\omega_{pe0} = 0.025(0.01)$ |
| Ion | $2v_{te0}(0.8v_{te0})$ | 500(512) | $-0.6v_{te0}(-0.4v_{te0})$ | $1.4v_{te0}(0.4v_{te0})$ | $t\omega_{pe0} = 400$ | $\Delta t\omega_{pe0} = 0.025(0.01)$ |

Table 3: Boundary Conditions for Semi-infinite(Finite-size) model

| | Left Bound | Right Bound |
|---|---|---|
| Poisson | Zero Dirichlet(Zero Neumann) | Zero Neumann |
| Vlasov(Spatial) | Fixed Value Dirichlet | Fixed Value Dirichlet |
| Vlasov(Velocity) | Fixed Value Dirichlet | Fixed Value Dirichlet |

# III. Results and Discussions

## A. Code Validation

We first validate the code using two classical problems, Landau damping and two-stream Instability.

### 1. *Linear Landau Damping*

A simulation is performed using periodic boundary condition to verify the code. Only one species, electron is considered in this simulation. The initial distribution function is given following the set-up in:[28]

$$\tilde{f} = \frac{1}{\sqrt{2\pi}} \exp\left(-\frac{\tilde{v}^2}{2}\right) \cdot (1 + \alpha \cos(kx)) \tag{13}$$

where $\alpha = 0.01$ and $k = 0.5$ and $v_{te0} = 1$. The domain is set to be periodic on the spatial domain and set to be cut off on velocity domain. The cut off limit for the velocity domain is set to be: $v_{\max} = 4.5v_{te0} = 4.5$, $v_{\min} = -4.5v_{te0} = -4.5$. The spatial domain is set to have a length of $4\pi$ and is divided into 32 cells. The velocity space is divided into 32, 64 cells respectively. Time step is set to be $\Delta\tilde{t} = \frac{1}{8}$. The plot of $\tilde{E}(t)$ versus of simulation time are shown below as figure 3a and 3b.

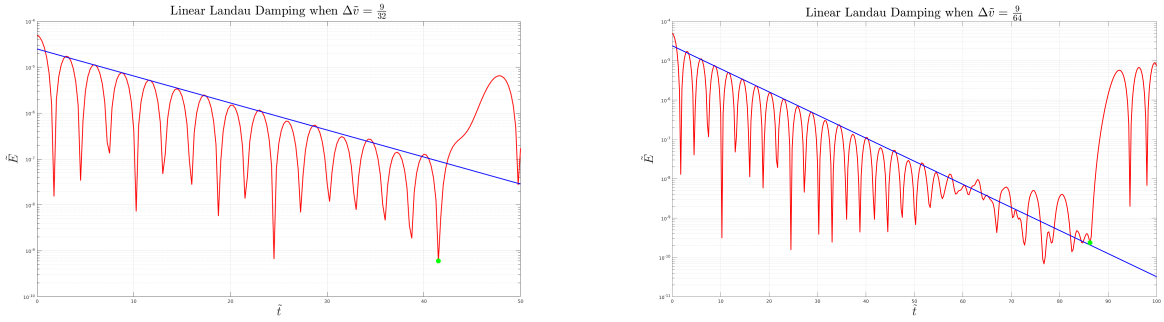


(a) $N_v$=32 (b) $N_v$=64

Figure 3: Linear Landau Damping with Different Velocity Cell Numbers

As predicted by the theory, the recurrence will happen at time $\tilde{T}_R = 2\pi/(k\Delta\tilde{v})$. Thus it can be easily found that the theory predict time for 32 velocity cells case should be $\tilde{T}_R = 44.86$ and for 64 cells case $\tilde{T}_R = 89.36$. It can be easily found from the simulation results that the recurrence happens near the predicted value. However, we need to note that the scheme will be less stable due to the less accurate electric field near the recurrence points.

### 2. *Two-Stream Instability*

The second validation is the two-stream instability problem. In the setup, two populations of electrons are included in this simulation. Both of the electrons are set to be in Maxwellian distribution at the start moment. One species is set to be "sit" in peace at the initial moment, namely, $\tilde{v}_d = 0$ at $\tilde{t} = 0$. The other species is set to be moving toward the sitting population with a drifting velocity $\tilde{v}_d = 5$ at $\tilde{t} = 0$. Velocity cut off limit for both populations are set to be $\tilde{v}_{\max} = 10$ and $\tilde{v}_{\min} = -10$. Both of two populations' initial thermal velocity are set to be $\tilde{v}_{te} = 1$. The contours of phase space evolution are shown in figure 4a and the plots for the evolution of distribution functions are shown in figure 4b.

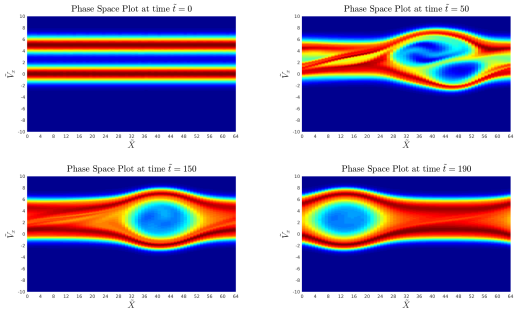


(a) Ion and Electron Phase Space Evolution

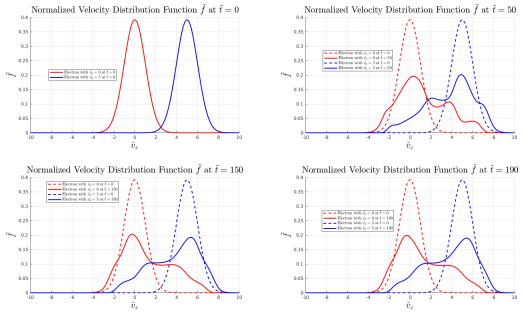


(b) Velocity Distribution Function Evolution

Figure 4: Two-Stream Instability

## B. Plasma Expansion Simulation

### 1. *Vlasov vs. PIC*

We first compare Vlasov with PIC on plasma diffusion simulation. Here, the mass ratio $m_i/m_e$ is 100 and the temperature ratio is $T_i/T_e = 1$. The initial density is $n_i/n_e = 1$.The initial plasma spatial distribution shown in figure 5a and the initial velocity distributions are shown in figure 5b. Two particle-in-cell simulations with

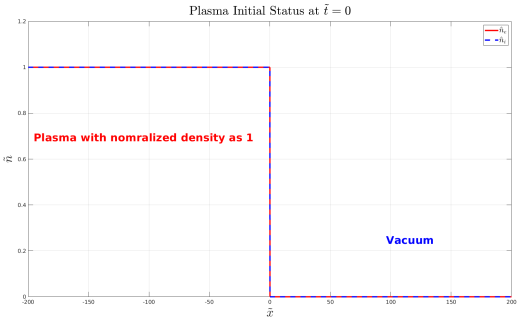


(a) Initial Plasma Spatial Distribution

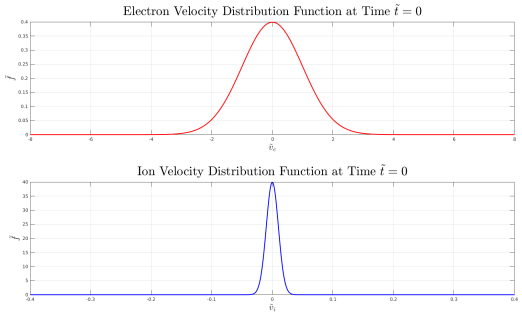


(b) Initial Plasma Velocity Distribution

Figure 5: Plasma Diffusion Simulation: Initial Condition

25600 particles per cell are used to perform simulations. First particle-in-cell simulation will be the results from one run and the second one will average the results from 36 runs. They are first compared with each other. The results for potential are shown below in figure 6a and figure 6b and results for temperature are shown in figure 6c and figure 6d.

The particle-in-cell methods resolve the velocity distribution functions by using macro particles. One macro particle can only represent $\tilde{f} \approx 1/N_p$ where $\tilde{f}$ is the normalized distribution function and $N_p$ is the number of particles used in the simulation.[38] In order to resolve the velocity distribution functions and reconstruct different moments of the distribution functions at the place where $\tilde{f}$ has a extremely low value,

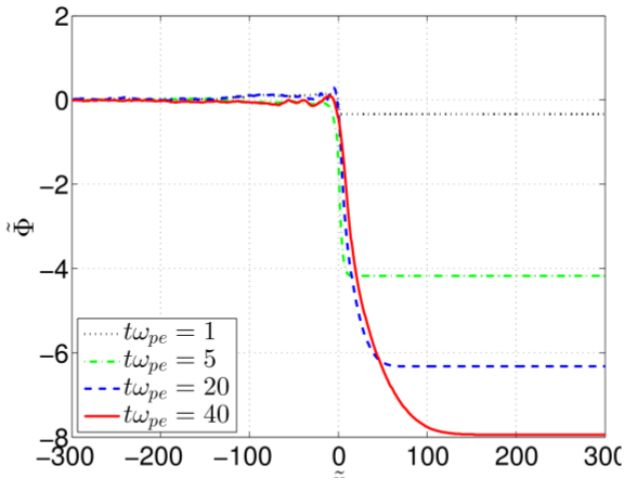


(a) Potential with 25600 Particles per Cell, 1 Run.

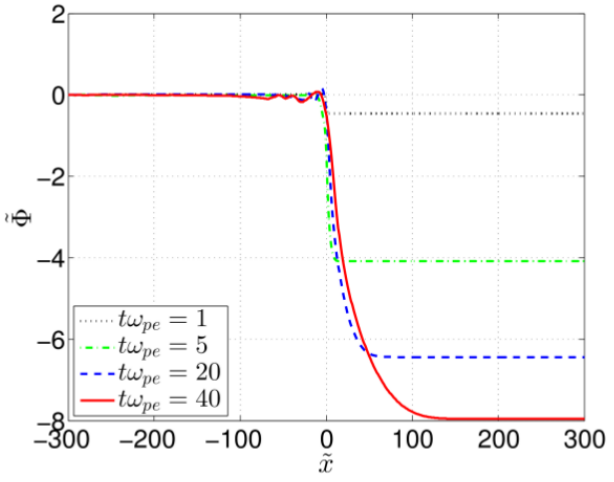


(b) Potential with 25600 Particles per Cell, 36 Runs Average

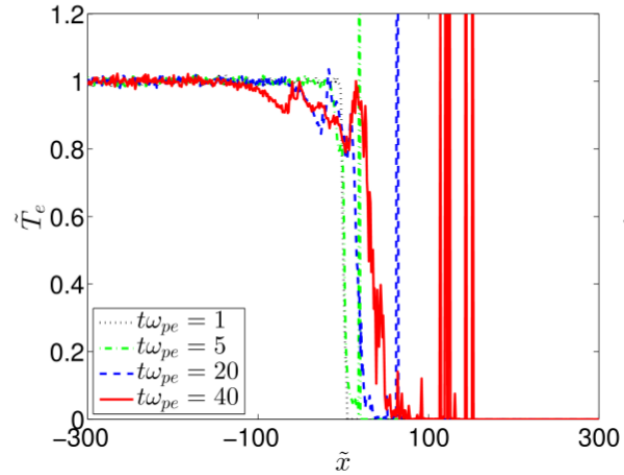


(c) Temperature with 25600 Particles per Cell, 1 Run

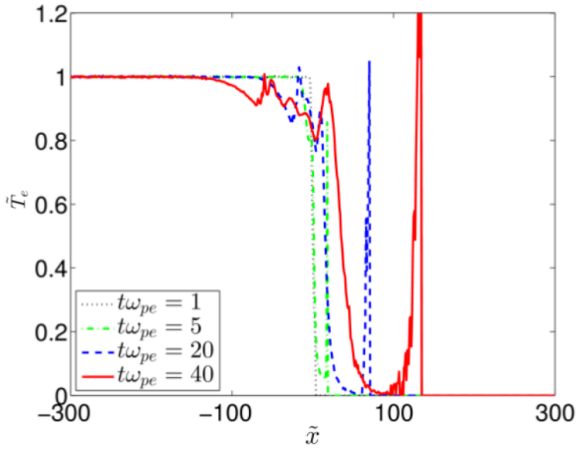


(d) Temperature with 25600 Particles per Cell, 36 Runs Average

Figure 6: Particle-in-cell Simulation Results for Plasma Diffusion

a large number of particles may need to be used. As shown in the figure 6, with the particles number increased, the noise will decrease. However, although a large number of particles are used, statistical noise still exist in the low density region and make it pretty hard to resolve the physics there. In other words, if one wants to resolve the physics in low-density region, which is pretty common in multi-scale problems in electric propulsion simulation, the particles number per cell may need to be a huge number and thus the computational cost required will be extremely big.

A grid-based Vlasov solver with 256 velocity bin cells and 4800 spatial bin cells is used for this problem. The results from this grid-based kinetic solver are compared with the particle-based method and presented in figure 7. The results suggest although in potential plot particle-in-cell method can reach a similar resolve ability with grid-based method, in the temperature plot which requires a high moment of velocity distribution function(VDF) the grid-based method can greatly reduce the numerical noise. In our work we would like to study the energy transfer process which is requires second order moments of the VDF so the grid-based method is proven to be a better method.

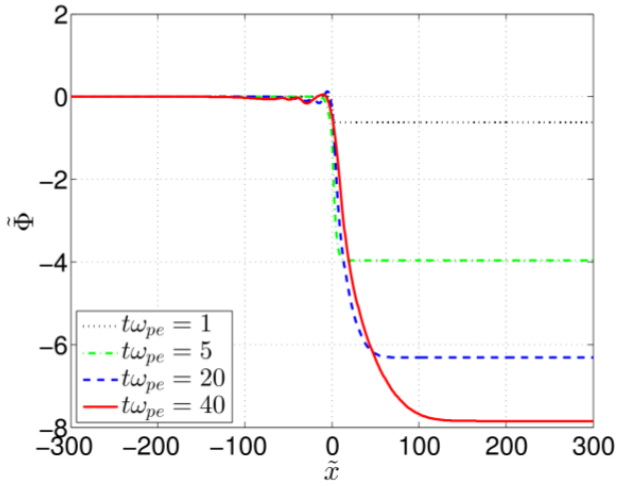


(a) Potential by using Grid-Based Kinetic Method

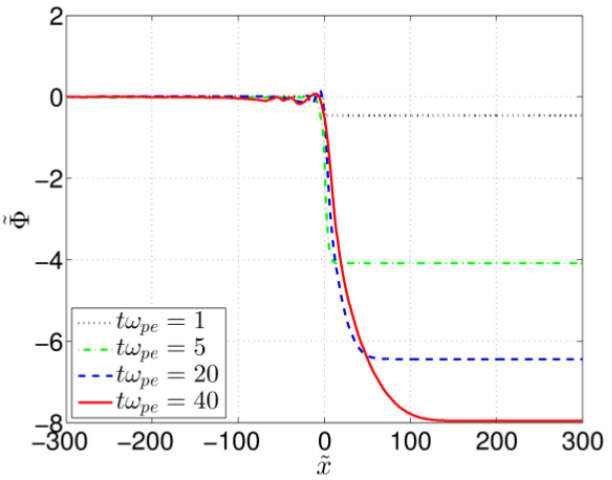


(b) Potential with 25600 Particles per Cell, 36 Runs Average

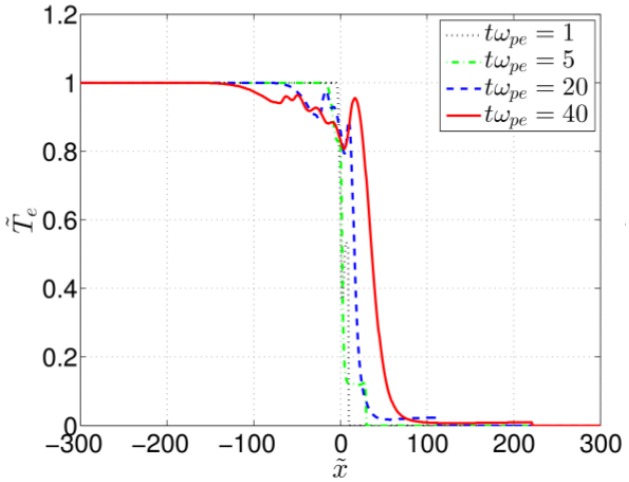


(c) Temperature by using Grid-Based Method

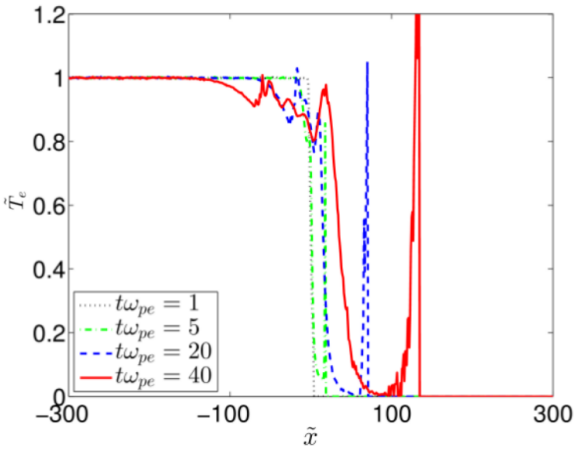


(d) Temperature with 25600 Particles per Cell, 36 Runs Average

Figure 7: Particle-in-cell and Vlasov Simulation Results for Plasma Diffusion

### 2. *Semi-Infinite Expansion*

Figures 8 and figure 9 show the evolution of phase space, and selected corresponding position's electron velocity distribution function. The snapshots plotted are taken at $\tilde{t} = 10$, $\tilde{t} = 50$, $\tilde{t} = 70$. $\tilde{t} = 250$. The temperature for the electrons and ions can be obtained by taking the moments of the velocity distribution function

$$\tilde{T}_\alpha = \tilde{m}_\alpha \cdot (< \tilde{v}^2 > - < \tilde{v} >^2) \tag{14}$$

We can then construct the local Maxwellian distribution

$$\tilde{f}_0 = \frac{1}{\sqrt{2\pi}\tilde{v}_{teL}} \exp(-\frac{(\tilde{v} - \tilde{v}_{bulk})^2}{\tilde{v}_{teL}^2}) \tag{15}$$

to compare against the actual velocity distribution The results show that the electron velocity distribution starts to deviate from the Maxwellian distribution immediately at the onset of the expansion. Subsequent interactions between the electrons and a potential well establish a new near-equilibrium for the electrons. This process is similar to that shown in previous full PIC simulations.

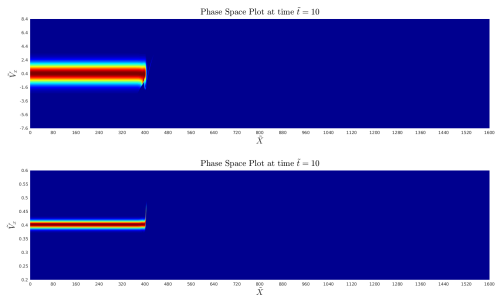


(a) Phase Space Contour at $\tilde{t} = 10$

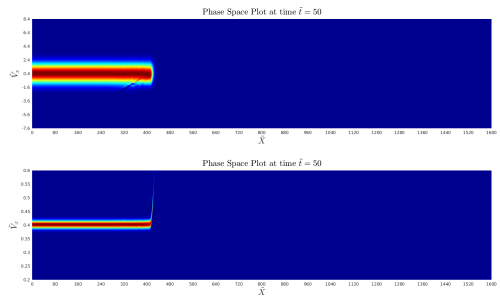


(b) Phase Space Contour at $\tilde{t} = 50$

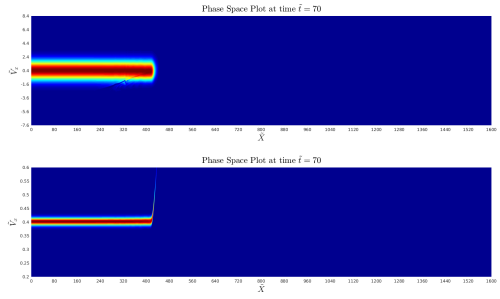


(c) Phase Space Contour at $\tilde{t} = 70$

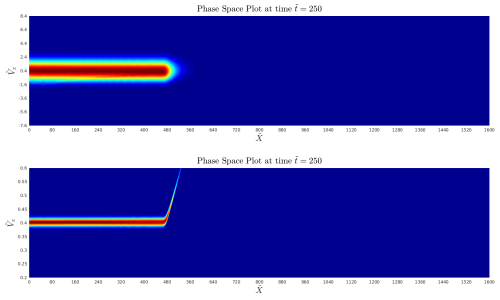


(d) Phase Space Contour at $\tilde{t} = 250$

Figure 8: Phase Space Evolution

Although the electrons physical processes are given concerns, the expansion of the plasma flow itself need to be studied in the scale of ion time scale. The simulation results up to 35 ion periods($t\omega_{pi} = 35$) were shown in this work. All of the simulations were run till 40 time periods to ensure that the results are still valid at a longer time moment. Figure 10 showed the electric potential profiles along the expansion direction's time evolution profile after the one-dimensional expansion is well developed. Three distinct regions can be observed in this figure: (1) unperturbed quasi-steady plasma region. (2) the self-similar expansion region and (3) The electron dominant front region.

The electric potential and plasma density will be in quasi-steady state in region (1): unperturbed region. Although rarefaction wave from expansion front will propagate through this region in the opposite of the plasma drifting's direction, In this region the "particles" rest with a near-equilibrium velocity distribution function. However, at the start of the expansion, the rarefaction waves generated from expansion front will introduce oscillations into this region and thus heat the electrons to the high energy tails as shown in the figure 8. The reason for such a phenomena can be explained as that when the rarefaction wave propagates upstream, the ion "particles" space will increase and thus electric field will be established between the ions and the unperturbed electrons. Such electric field will then drive the electrons for oscillations and result in the deviations of the electrons in phase plot. Such small oscillations can also be observed in the density plot.

Next to the unperturbed region is the self-similar expansion region. In the previous theoretical work of semi-infinite plasma expansion studies,[8–11] self-similar solutions of a stationary plasma expansion can be obtained with an assumption of quasi-neutrality and isothermal electrons. In this work fully grid-based kinetic simulations are performed on the drifting semi-infinite expansion to identify the validity region of the self-similar solutions. The transition point between the region (1) and region (2) propagates along the expansion drifting direction with a quasi-constant speed which corresponds to the results generated by the self-similar solution. The vertical segmentation lines can be obtained from the self-similar solutions' predictions on expansion propagations. However, one should note that as the model is drifting along the x direction, the propagation speed of the expansion should be modified to $v_0 - C_s$ as discussed in Hu and

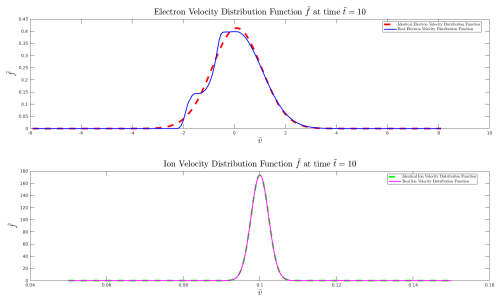


(a) Distribution Function Plot at $\tilde{t} = 10$

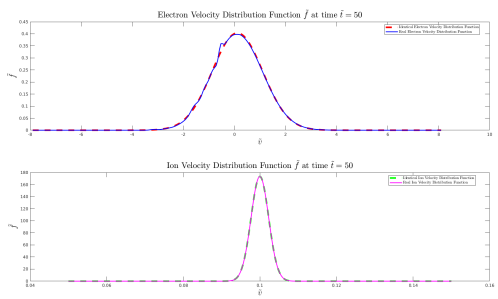


(b) Distribution Function Plot at $\tilde{t} = 50$

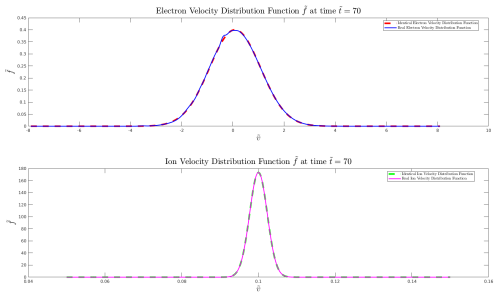


(c) Distribution Function Plot at $\tilde{t} = 70$

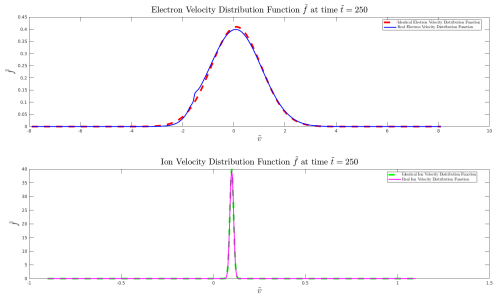


(d) Distribution Function Plot at $\tilde{t} = 250$

Figure 9: Evolution of Velocity Distribution Function

Wang's previous work.[7] Thus the control equation for the segmentation lines should be

$$\tilde{x} = t\omega_{pi} M_{eff} + \tilde{x}_o \tag{16}$$

in which the $M_{eff}$ is the effective Mach number which can be obtained by $M_{eff} = v_0/C_s - 1$. On the right hand side of the segmentation line is the region (2). It is clear that in this region the potential plot has a quasi-linear decrease. In the previous self-similar theoretical work,[8] it had been found that the potential is proportional to the distance as $\tilde{\Phi} = -1 - \tilde{x}/t\omega_{pi}$. Thus the value for $d\Phi/dx$ should be a constant of $-1/t\omega_{pi}$. It can be observed from the figure 10 that the slope of potential plot in the region paralleled with dotted lines is approximately equal to $-1/t\omega_{pi}$. It can be thus identified that the self-similar solution is valid in this region.

From the figure 10, it can be observed there is a curve shape potential drop and this drop region will at last approximate a constant value. This region is identified as the electron dominant front region. In this region the quasi-neutral assumption can not be hold anymore and the electrons will be the dominant species inside. This can also be observed in the phase plot contour. This charge separation effects can be a divide feature to distinguish region (2) and region (3) and the self-similar solution are not suitable in this region.

Thermodynamics properties of the expansion model is studied. Density of both ions and electrons together with electron temperature are plotted in the same figure as a reference for discussions late in the left hand side of the figure 11. As the polytropic law can be written as

$$\frac{\tilde{T}_e}{\tilde{n}_e^{\gamma-1}} = C \tag{17}$$

the $\log_{10}(\tilde{T}_e)$ to $\log_{10}(\tilde{n}_e)$ relation will be studied and the results are shown in the right hand side of the figure 11. According to equation (17), the slope of the plotted line in the figure can be identified as $k = \gamma - 1$. Here we use the notation $\delta\gamma = \gamma - 1$ to represent the slope's value. It can be observed that in right up plot of figure 11, there is a small vertical tail region. This region correspond to the unperturbed region mentioned above. In this region the density will have a value around $\tilde{n}_e = 1$ since the plasma is injected

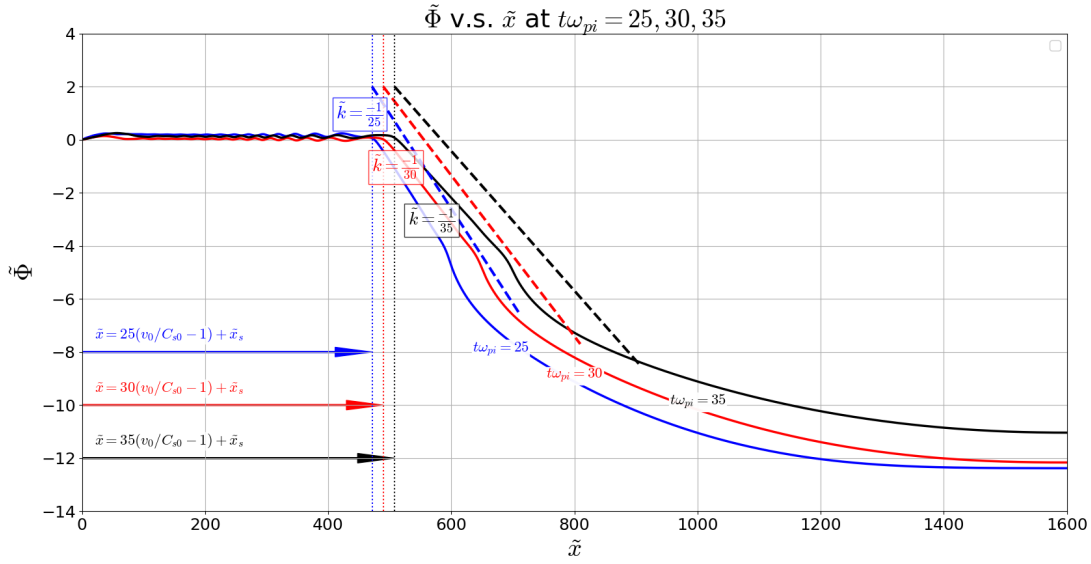


Figure 10: Electric Potential Plot at Different Time Moment

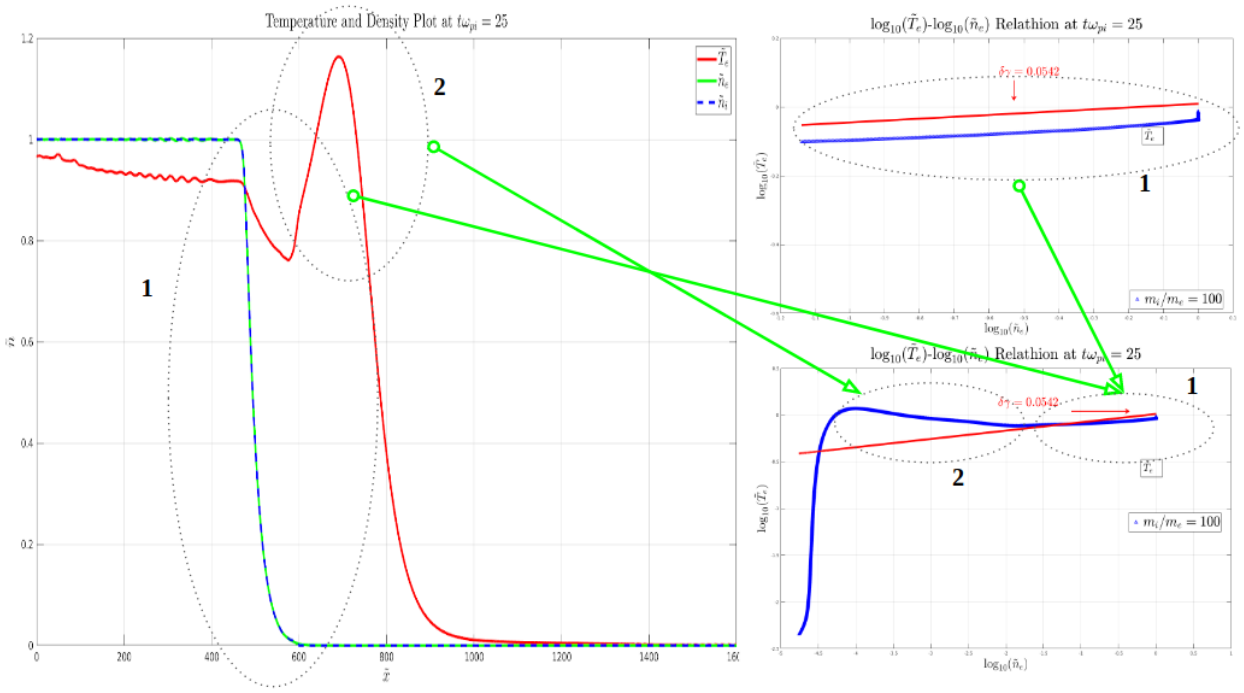


Figure 11: Left: Density and Temperature Plot. Right Up: Zoomed In $\log_{10}(\tilde{T}_e) - \log_{10}(\tilde{n}_e)$ Relation. Right Down: Global $\log_{10}(\tilde{T}_e) - \log_{10}(\tilde{n}_e)$ Relation

indefinitely from left boundary side. The temperature as shown in left hand side of figure 11 will have a slight drop. The reason for the slight drop can be resulted from the perturbations received from expansion front. The dotted circle region 1 denotes the expansion front where the self-similar solution can be used. It can be observed in the dotted circle region 1 in right hand side plots that in this region a linear relationship is formed between $\log_{10} \tilde{T}_e$. The slope of an approximation line to this region is $k = \delta\gamma = 0.0542 \approx 0$.

This process can be approximately treated as an quasi-isothermal process and the self-similar solution by taking the isothermal electron assumption will be valid in this region. The reason for such a process can be explained as that the energy is feed in the system without stop from left-hand side as this is a semi-infinite plasma model. Although the electrons will be cooled down during the expansion process, the energy loss will be supplied from the injected plasma. The temperatures profiles in the dotted circle region 2 is interesting. It can be found that in the left hand side plot of figure 11, there exist a temperature peak ahead of the expansion front. This part is circled by the dotted region 2. It can be found in the right down plot of figure 11, the approximate slope for the $\log - \log$ plot is negative. The negative value means that the temperature increase while the density decrease. As shown in the phase space plot and velocity distribution function plot above, the velocity distribution function deviate from Maxwellian distribution. Temperature used here is a derivation of the second moment of the velocity distribution function, and in the non-equilibrium region the change of the kinetic temperature can not respond to the macroscopic so-called heating or cooling as discussed in Hu and Wang's previous work.[39] As shown in the distribution function, the electrons' velocity distribution function density at the high-energy tail. This may result in the temperature peak shown in the figure 11.

### *3. Finite-Size Expansion*

Figures 12 and 13 show the evolution of density and phase space, respectively. The phase plot shows that the electrons are non-equilibrium during the expansion process. The electrons are driven to the high energy tail by the potential well established in the expansion front.

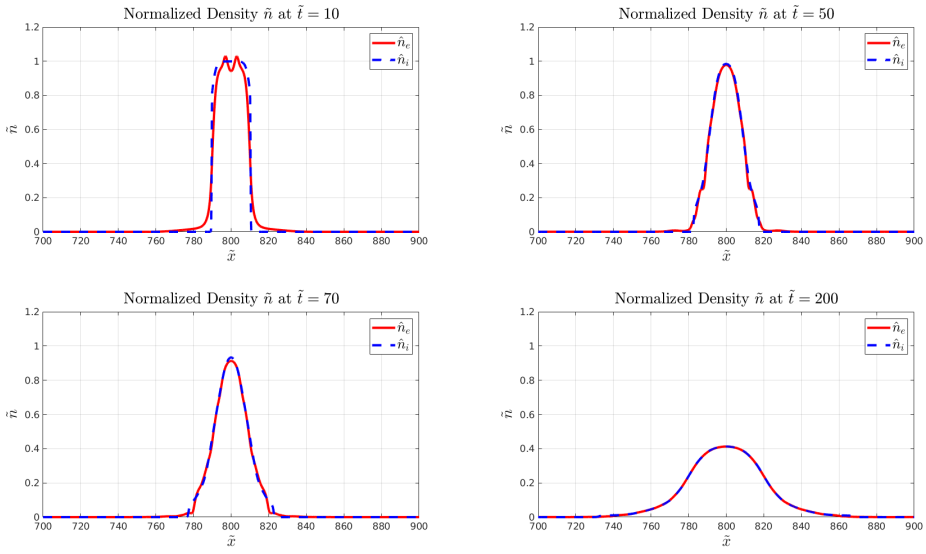


Figure 12: Density Evolution

Thermodynamics properties are studied for finite-size model and the results are presented in figure 14. It can be observed from the previous phase space plot and the density plot that the characteristics of the finite-size model is different with the semi-infinite model. In the semi-infinite model the energy can be provided unlimitedly since the plasma was injected though the left hand domain continuously. However, in the finite-size model, the amount of plasma is limited and thus the electron energy has a finite amount. The expansion is driven by the loss of the electrons' energy. In this way the electrons energy evolution plays an important role. As shown in the figure 14, the temperature and density construct a linear relation in the $\log - \log$ plot in the circle dotted region 1. The approximate line's slope is equal to $\delta\gamma = 0.9880 \approx 1$. As discussed in the classical thermodynamics, the adiabatic constant $\delta\gamma$ for one dimensional system should be equal to 2. The reason for the difference between these two values may result from the electrons' distribution functions equilibrium status. The classical results are derived from the equilibrium state which may not be satisfied in this region. Outside the dotted circle region 1 the temperature shown un-classical behavior. As

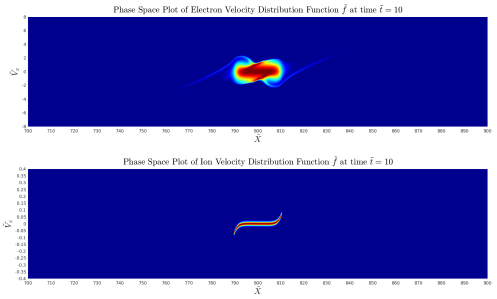


(a) Phase Space Contour at $\tilde{t} = 10$

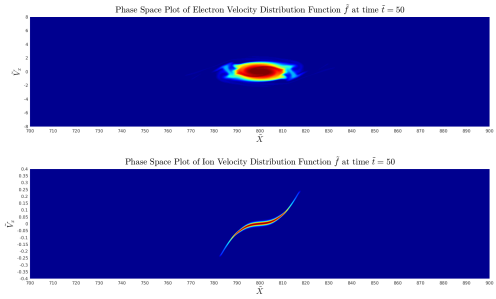


(b) Phase Space Contour at $\tilde{t} = 50$

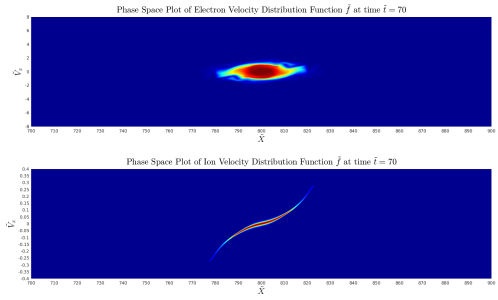


(c) Phase Space Contour at $\tilde{t} = 70$

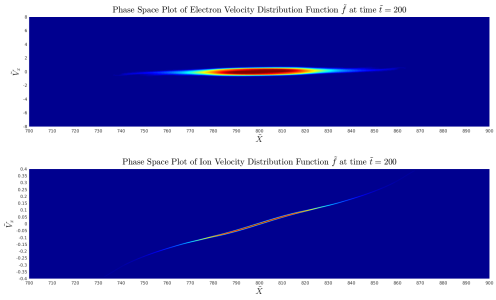


(d) Phase Space Contour at $\tilde{t} = 200$

Figure 13: Phase Space Evolution

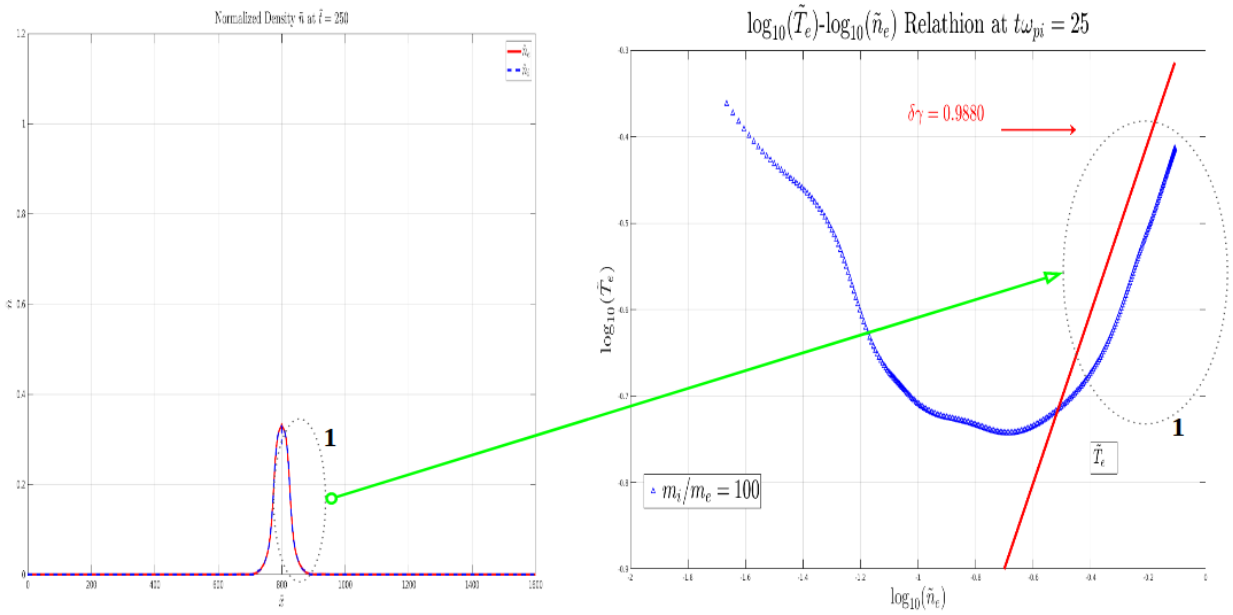


Figure 14: Left: Density Plot. Right: $\log_{10}(\tilde{T}_e) - \log_{10}(\tilde{n}_e)$ Relation.

the density decrease the temperature increase. In such region the polytropic law can not give a good fit and it has been found that the polytropic fit can only be used before the expansion front. The reason for the non-trivial temperature behavior needs to be investigated further.

## IV. Conclusion

Previous fully kinetic PIC simulations showed that the electrons in the plasma plume emitted from electric propulsion thrusters are non-equilibrium and the electron temperature is anisotropic. A grid-based Vlasov method model is developed in this work to further study the electron kinetic properties in plasma expansion and to reduce the interference from numerical noise in particle simulations. This model is benchmarked against particle-in-cell simulations and analytical solutions on semi-infinite collisionless plasma expansion and finite-size collisionless plasma expansion. It is shown that the Vlasov model captures the same kinetic characteristics observed in previous full PIC simulation results and eliminates the interference from the typical numerical noise in a PIC model. An analysis is presented to study the thermodynamics properties of two models. It has been found that the isothermal relationship can be a good fit for describing the relation between electron temperature and density in the self-similar region of semi-infinite model and the polytropic model can be used for the region before expansion front in finite-size model. Outside these regions the polytropic law breaks down and further details need to be studied by using kinetic model.Future efforts will extend the model to 2D2V so it can applied to simulate the actual plume problem. Further studies will also need to investigate the relation between the thermodynamics properties observed and electron energy transport inside the plume.

## References


[1]RI Samanta Roy, DE Hastings, and NA Gastonis. Ion-thruster plume modeling for backflow contamination. *Journal of Spacecraft and Rockets*, 33(4):525–534, 1996.

[2]J Wang, D Brinza, and M Young. Three-dimensional particle simulations of ion propulsion plasma environment for deep space 1. *Journal of Spacecraft and Rockets*, 38(3):433–440, 2001.

[3]Burak Korkut and Deborah A Levin. Three-dimensional simulations of backflows from ion thruster plumes using unstructured grid refinement. *Journal of Propulsion and Power*, pages 264–275, 2016.

[4]Filippo Cichocki, Adrián Domínguez-Vázquez, Mario Merino, and Eduardo Ahedo. Hybrid 3d model for the interaction of plasma thruster plumes with nearby objects. *Plasma Sources Science and Technology*, 26(12):125008, 2017.

[5]Yuan Hu and Joseph Wang. Electron properties in collisionless mesothermal plasma expansion: Fully kinetic simulations. *IEEE Transactions on Plasma Science*, 43(9):2832–2838, 2015.

[6]Yuan Hu and Joseph Wang. Fully kinetic simulations of collisionless, mesothermal plasma emission: Macroscopic plume structure and microscopic electron characteristics. *Physics of Plasmas*, 24(3):033510, 2017.

[7]Yuan Hu and Joseph Wang. Expansion of a collisionless hypersonic plasma plume into a vacuum. *Physical Review E*, 98(2):023204, 2018.

[8]AV Gurevich, LV Pariiskaya, and LP Pitaevskii. Self-similar motion of rarefied plasma. *Sov. Phys. JETP*, 22(2):449–454, 1966.

[9]JE Allen and JG Andrews. A note on ion rarefaction waves. *Journal of Plasma Physics*, 4(1):187–194, 1970.

[10]JE Crow, PL Auer, and JE Allen. The expansion of a plasma into a vacuum. *Journal of Plasma Physics*, 14(1):65–76, 1975.

[11]J Denavit. Collisionless plasma expansion into a vacuum. *The Physics of Fluids*, 22(7):1384–1392, 1979.

[12]Patrick Mora and R Pellat. Self-similar expansion of a plasma into a vacuum. *The Physics of Fluids*, 22(12):2300–2304, 1979.

[13]Patrick Mora. Plasma expansion into a vacuum. *Physical Review Letters*, 90(18):185002, 2003.

[14]G Manfredi, S Mola, and MR Feix. Rescaling methods and plasma expansions into vacuum. *Physics of Fluids B: Plasma Physics*, 5(2):388–401, 1993.

[15]T Grismayer, P Mora, JC Adam, and A Héron. Electron kinetic effects in plasma expansion and ion acceleration. *Physical Review E*, 77(6):066407, 2008.

[16]P Mora and T Grismayer. Rarefaction acceleration and kinetic effects in thin-foil expansion into a vacuum. *Physical review letters*, 102(14):145001, 2009.

[17]AV Baitin and KM Kuzanyan. A self-similar solution for expansion into a vacuum of a collisionless plasma bunch. *Journal of Plasma physics*, 59(1):83–90, 1998.

[18]DS Dorozhkina and VE Semenov. Exact solution of vlasov equations for quasineutral expansion of plasma bunch into vacuum. *Physical review letters*, 81(13):2691, 1998.

[19]Patrick Mora. Thin-foil expansion into a vacuum. *Physical Review E*, 72(5):056401, 2005.

[20]P Mora. Collisionless expansion of a gaussian plasma into a vacuum. *Physics of plasmas*, 12(11):112102, 2005.

[21]M Murakami and MM Basko. Self-similar expansion of finite-size non-quasi-neutral plasmas into vacuum: Relation to the problem of ion acceleration. *Physics of plasmas*, 13(1):012105, 2006.

[22]T Grismayer and P Mora. Influence of a finite initial ion density gradient on plasma expansion into a vacuum. *Physics of Plasmas*, 13(3):032103, 2006.

[23]Chio-Zong Cheng and Georg Knorr. The integration of the vlasov equation in configuration space. *Journal of Computational Physics*, 22(3):330–351, 1976.

[24]James A Rossmanith and David C Seal. A positivity-preserving high-order semi-lagrangian discontinuous galerkin scheme for the vlasov–poisson equations. *Journal of Computational Physics*, 230(16):6203–6232, 2011.

[25]Jeffrey William Banks and Jeffrey Alan Furst Hittinger. A new class of nonlinear finite-volume methods for vlasov simulation. *IEEE Transactions on Plasma Science*, 38(9):2198–2207, 2010.

[26]Nina V Elkina and Jörg Büchner. A new conservative unsplit method for the solution of the vlasov equation. *Journal of Computational Physics*, 213(2):862–875, 2006.

[27]Jing-Mei Qiu and Andrew Christlieb. A conservative high order semi-lagrangian weno method for the vlasov equation. *Journal of Computational Physics*, 229(4):1130–1149, 2010.

[28]Francis Filbet, Eric Sonnendrücker, and Pierre Bertrand. Conservative numerical schemes for the vlasov equation. *Journal of Computational Physics*, 172(1):166–187, 2001.

[29]Takayuki Umeda, Yasuhiro Nariyuki, and Daichi Kariya. A non-oscillatory and conservative semi-lagrangian scheme with fourth-degree polynomial interpolation for solving the vlasov equation. *Computer Physics Communications*, 183(5):1094–1100, 2012.

[30]Jing-Mei Qiu and Chi-Wang Shu. Positivity preserving semi-lagrangian discontinuous galerkin formulation: theoretical analysis and application to the vlasov–poisson system. *Journal of Computational Physics*, 230(23):8386–8409, 2011.

[31]Yasuhiro Idomura, Tomo-Hiko Watanabe, and Hideo Sugama. Kinetic simulations of turbulent fusion plasmas. *Comptes Rendus Physique*, 7(6):650–669, 2006.

[32]AGR Thomas, M Tzoufras, APL Robinson, RJ Kingham, CP Ridgers, Mark Sherlock, and AR Bell. A review of vlasov–fokker–planck numerical modeling of inertial confinement fusion plasma. *Journal of Computational Physics*, 231(3):1051–1079, 2012.

[33]Takayuki Umeda, Tetsuya Kimura, Kentaro Togano, Keiichiro Fukazawa, Yosuke Matsumoto, Takahiro Miyoshi, Naoki Terada, Takuma KM Nakamura, and Tatsuki Ogino. Vlasov simulation of the interaction between the solar wind and a dielectric body. *Physics of Plasmas*, 18(1):012908, 2011.

[34]Minna Palmroth, Urs Ganse, Yann Pfau-Kempf, Markus Battarbee, Lucile Turc, Thiago Brito, Maxime Grandin, Sanni Hoilijoki, Arto Sandroos, and Sebastian von Alfthan. Vlasov methods in space physics and astrophysics. *Living reviews in computational astrophysics*, 4(1):1, 2018.

[35]Kentaro Hara, Iain D Boyd, and Vladimir I Kolobov. One-dimensional hybrid-direct kinetic simulation of the discharge plasma in a hall thruster. *Physics of Plasmas*, 19(11):113508, 2012.

[36]Petr Cagas, Bhuvana Srinivasan, and Ammar Hakim. Continuum kinetic study of magnetized sheaths for use in hall thrusters. In *52nd AIAA/SAE/ASEE Joint Propulsion Conference*, page 4619, 2016.

[37]Satoshi Tanaka, Kohji Yoshikawa, Takashi Minoshima, and Naoki Yoshida. Multidimensional vlasov–poisson simulations with high-order monotonicity-and positivity-preserving schemes. *The Astrophysical Journal*, 849(2):76, 2017.

[38]Kentaro Hara. High-energy ion generation due to the plasma wave driven by current-carrying instabilities. In *AIAA Propulsion and Energy 2019 Forum*, page 4249, 2019.

[39]Yuan Hu and Joseph Wang. Assessment of electron thermodynamic and fluid approximations for collisionless plasma expansion into a wake. *Physics of Plasmas*, 26(2):023515, 2019.